# RSC Sustainability

Accepted Manuscript

Published on 05 August 2026




This is an Accepted Manuscript, which has been through the Royal Society of Chemistry peer review process and has been accepted for publication.

Accepted Manuscripts are published online shortly after acceptance, before technical editing, formatting and proof reading. Using this free service, authors can make their results available to the community, in citable form, before we publish the edited article. We will replace this Accepted Manuscript with the edited and formatted Advance Article as soon as it is available.

You can find more information about Accepted Manuscripts in the Information for Authors.

Please note that technical editing may introduce minor changes to the text and/or graphics, which may alter content. The journal's standard Terms & Conditions and the Ethical guidelines still apply. In no event shall the Royal Society of Chemistry be held responsible for any errors or omissions in this Accepted Manuscript or any consequences arising from the use of any information it contains.


ROYAL SOCIETY OF CHEMISTRY

**Sustainability Spotlight Statement**

This study delivers sustainable advancements by generating designer enzymatic hydrolysates from Miscanthus, a renewable energy crop, producing optimized fermentable sugar streams (up to 173.4 g/L xylose and 127.7 g/L glucose) while minimizing inhibitory by-products. The process preserves high-lignin residues (73.7 to 85.7%) for sustainable valorization, enabling complete biomass valorization and waste reduction. This directly aligns with UN SDG 7 (Affordable and Clean Energy) through renewable biofuel production, SDG 9 (Industry, Innovation and Infrastructure) via integrated biorefinery platforms, SDG 12 (Responsible Consumption and Production) through circular resource recovery, and SDG 13 (Climate Action) by replacing fossil-derived products with bio-based alternatives. By achieving lipid yields up to 41.7 g/kg biomass this work enables eco-efficient bioproduct manufacturing supporting the transition to a circular bioeconomy.

# Selective designer hydrolysates from Miscanthus bioenergy crop for sustainable utilization

Shuchi Singh[ab], Tirath Raj[ab], Joshua Ye[ac], Sujit Sadashiv Jagtap[ac], Cindy Yang [ac], Christopher V. Rao[ac], Vijay Singh[ab*]

[a]DOE Center for Advanced Bioenergy and Bioproducts Innovation (CABBI), University of Illinois at Urbana-Champaign, Urbana, IL 61801, USA
[b]Department of Agricultural and Biological Engineering, University of Illinois Urbana-Champaign, Urbana, IL 61801, USA
[c]Department of Chemical and Biomolecular Engineering, University of Illinois Urbana-Champaign, Urbana, IL 61801, USA

***Corresponding author:**
DOE Center for Advanced Bioenergy and Bioproducts Innovation (CABBI), University of Illinois at Urbana-Champaign, Urbana, IL 61801, USA
Department of Agricultural and Biological Engineering, University of Illinois Urbana-Champaign, 1304 W Pennsylvania Ave, Urbana, IL 61801, USA
e-mail: vsingh@illinois.edu

## List of Abbreviations:

| | | |
|---|---|---|
| ACL | : | ATP-citrate lyase |
| AIL | : | Acid insoluble lignin |
| AMP | : | Adenosine Monophosphate |
| ASL | : | Acid soluble lignin. |
| AXE | : | Acetylxylan Esterase |
| C/N | : | Carbon-to-Nitrogen ratio |
| CRF | : | Cellulose-rich fraction (CRF), |
| CRF-EH | : | Cellulose rich fraction-Enzymatic hydrolysate |
| CRI | : | Crystallinity index |
| EH | : | Enzymatic hydrolysates |
| FAMEs | : | Fatty acid methyl esters |
| FT-IR | : | Fourier transform infrared |
| GC-FID | : | Gas chromatography-flame-ionization detection |
| HM-A | : | Hemicellulose A |
| HM-B | : | Hemicellulose B |
| HMR | : | Hydrothermal-mechanical refining |
| HMR-EH1 | : | Hydrothermal-mechanical refining-Enzymatic hydrolysate 1 |
| HMR-EH2 | : | Hydrothermal-mechanical refining-Enzymatic hydrolysate 2 |
| HMR-EH2* | : | Hydrothermal-mechanical refining-Enzymatic hydrolysate 2, C/N adjusted to half |
| HMA-EH | : | Hemicellulose A-Enzymatic hydrolysate |
| HMB-EH | : | Hemicellulose B-Enzymatic hydrolysate |
| HMB-EH* | : | Hemicellulose B-Enzymatic hydrolysate, C/N adjusted to half |
| HPLC | | High-performance liquid chromatography |
| HSQC-NMR | : | Heteronuclear Single-Quantum Coherence-Nuclear Magnetic Resonance |
| M×g | : | Miscanthus × giganteus |
| *R. toruloides* | : | *Rhodotorula toruloides* |
| TCA cycle | : | Tricarboxylic Acid cycle |
| XRD | : | X-ray diffraction |

**Abstract**

Designer enzymatic hydrolysates deliver targeted, optimized fermentable sugars while reducing the formation of inhibitory by-products. Herein, five distinct enzymatic hydrolysates (EH) were generated from Miscanthus biomass using an alkaline-ethanol fractionation and hydrothermal-mechanical refining (HMR) pretreatment approaches. Noticeably, alkali-ethanol fractionated hemicellulose A (HMA) and hemicellulose B (HMB) hydrolysis resulted in xylose-rich enzymatic hydrolysates with 104.8 ± 5.6 g/L and 173.4 ± 4.6 g/L xylose, respectively. All five hydrolysates encompassing varied carbon to nitrogen ratio were evaluated for lipid production using an engineered oleaginous yeast, *R. toruloides* 880-ADS. Microbial fermentation of xylose-rich hydrolysates, *viz*. HMR-EH2, HMA-EH, and HMB-EH resulted in lipid yields ranging from 0.05 to 0.12 g/g sugar. Compositional and 2D NMR analysis revealed that HMA-EH residues are highly lignin-enriched, while preserving the non-condensed structure conducive to valorization. Overall, findings highlighted a novel, selective trade-offs approach for maximizing lipid titers from designer hydrolysates, corroborating complete resource recovery for establishing integrated biorefineries.

**Keywords:** Hemicellulose isolation, Xylose-rich hydrolysates, Lignin, *Rhodotorula toruloides*, Lignocellulosic biomass

## 1. Introduction

Miscanthus × giganteus (M×g) is a perennial crop with high photosynthetic efficiency and effective nutrient and water use, adaptable to diverse climates [1]. It is rich in cellulose (40%), hemicellulose (20%), and lignin (20%), which can be converted into bioethanol, biogas, microbial lipids, and biopolymers via enzymatic hydrolysis and fermentation [2]. Enzymatic hydrolysis breaks down complex polysaccharides into simple sugars for fermentation. Hemicellulose, the second most abundant carbohydrate after cellulose, has a complex structure that limits its industrial use [3]. Innovative biomass valorization is needed to fully exploit these carbohydrates' industrial potential.

Bioconversion of lignocellulose into hexose and pentose sugars is essential for biofuels and chemicals [4,5]. Enzymatic hydrolysis is limited by polymerization, crystallinity, and complex linkages in cellulose, hemicellulose, and lignin [6]. Pretreatments *viz*., physical, chemical, physicochemical, or biological, improve digestibility by breaking biomass recalcitrant structure [7]. Hydrothermal pretreatment with mechanical refining (HMR) applied to oilcane, energy cane, and M×g preserved lipids or recovered anthocyanins but did not separate biomass components [8,9]. Fractionation creates designer hydrolysates enriched in sugars like xylose, favored by engineered microbes for producing high-value fermentation products [10]. Such microbes often perform better on non-traditional carbon sources like xylose than on glucose, which is preferentially metabolized via native pathways. Therefore, designer hydrolysates enriched in xylose from cellulosic feedstocks are advantageous for producing novel high-value fermentation products by engineered microorganisms. Xylan makes up to 40% of structural carbohydrates in cellulosic feedstocks, yet only few pretreatments effectively separate cellulose, hemicellulose, and lignin [11]

Alkaline pretreatment, a common and eco-friendly method, uses chemicals like ammonia, sodium carbonate, calcium hydroxide, and especially sodium hydroxide (NaOH) for lignin removal in biomass processing [6]. NaOH breaks ester linkages between hemicellulose and lignin, swelling cellulose and enhancing enzyme accessibility [12]. The effectiveness of alkaline pretreatment extends beyond delignification, as it has been shown to isolate hemicelluloses, cellulose, and significantly enhance biofuel production in subsequent bioconversion processes [13,14]. Enzymatic hydrolysis converts these fractions into xylose and glucose hydrolysates, ideal for engineered microbes that transform xylose into organic acids, alcohols, lipids, biohydrogen, and other compounds [15]. Glucose-xylose-acetic acid hydrolysates can be utilized to assess the performance of recombinant microorganisms engineered to co-utilize these lignocellulose-derived substrates [16,17]. Though acetic acid is often inhibitory, engineered *Saccharomyces cerevisiae* can co-utilize xylose and acetic acid for biofuel and nutrient production, enabling innovative bioprocesses and improving lignocellulosic biorefinery economics [4,18]. This breakthrough enables innovative bioprocess designs to optimize sugar and organic acid production, improving lignocellulosic biorefinery economics. Generating separate sugar streams allows targeted bioconversion and expands bio-based product development opportunities.

Among various valuable compounds from biomass components, the microbial lipids hold significant promise for various applications, including biofuel production and as precursors in the synthesis of bioplastics and other industrial chemicals [19]. *Rhodotorula toruloides*, an oleaginous yeast, can efficiently accumulate lipids from sugars when cultivated in nitrogen-limited media [20]. *R. toruloides* can grow on diverse carbon sources, including plant sugars, lignocellulosic hydrolysates, organic acids and lignin-derived aromatics [20]. *R. toruloides* can natively produce arabitol and galactitol from xylose and galactose, respectively [19].

This study demonstrates a selective trade-offs strategy for fractionating Miscanthus × giganteus biomass using parallel pretreatments, alkaline-ethanol fractionation and HMR to generate compositionally distinct designer enzymatic hydrolysates enriched in either glucose or xylose. By integrating enzymatic hydrolysis, microbial lipid fermentation with engineered *R. toruloides* 880-ADS, and lignin characterization of spent residues, this integrated cascade maximizes both pentose-to-lipid conversion and lignin valorization potential. To our knowledge, this is the first report of systematically producing selective designer hydrolysates from Miscanthus to evaluate strain-specific sugar utilization patterns while enabling complete resource recovery, establishing a blueprint for sustainable, profitable lignocellulosic biorefineries.

## 2. Materials and methods

### 2.1. Miscanthus × giganteus biomass and compositional analysis

Miscanthus × giganteus (M×g), a triploid genotype 'Illinois' was cultivated in experimental field plots at the University of Illinois Energy Farm in Urbana, Illinois, USA. The plant biomass was harvested in February 2024, and during the harvest, the biomass was shredded and subsequently dried in a convection air oven at 49 °C until the moisture was < 5% (w/w). For biomass fractionation by alkaline pretreatment, dried biomass was milled to 0.5 mm using a hammer mill (W-8-H Schutte-Buffalo, Buffalo, NY, USA), packaged, and stored at 4 °C. To compare digestibility and explore applications beyond anthocyanin extraction, HMR pretreated M×g biomass was evaluated against raw M×g as a baseline [8]. Glucan, xylan, and lignin compositions of raw, pretreated, and fractionated samples were determined using NREL Laboratory Analytical Procedures (LAP) protocols [21]. Biomass moisture was kept below 10%. Extractives were removed by sequential Soxhlet extraction with hexane, water, and ethanol (4 h

each) and reported as percent extractives. The extractive-free biomass (300 mg) was digested using a two-step 72% $H_2SO_4$ hydrolysis to quantify total carbohydrates. Samples were analyzed for extractives, glucan, xylan, acetic acid, lignin (acid-insoluble lignin-AIL and acid-soluble lignin-ASL), and ash contents.

**2.2. Oleaginous yeast strain, culture medium, and enzymes**

*R. toruloides* 880-ADS (RT-ADS), derived from wild-type IFO0880 (genotype: IFO0880/$P_{GAPDH}$ -ACC1-$T_{ACC1}$-$P_{ACL}$-DGA1-$T_{DGA1}$-pGI2H-SCD), was engineered for improved lipid production [22]. Frozen stock was streaked on YPD agar with nourseothricin and hygromycin B (100 µg/mL each), incubated at 30 °C for 2-3 days. Single colonies were grown in YNBD medium (1.7 g/L yeast-nitrogen base without amino acids, 5 g/L ammonium nitrate, and 20 g/L glucose, pH 7.0) for 2 days. The lipid production medium was supplemented with specific hydrolysates and ammonium nitrate to adjust the carbon-to-nitrogen (C/N) ratio as needed. The C/N ratio of each hydrolysate was determined by CHN elemental analysis and, where feasible, was adjusted to the desired level. This approach enabled assessment of the effect of C/N ratio on lipid accumulation. The composition of the hydrolysate medium is described in Section 2.6. Fermentation experiments were carried out in 20 mL of hydrolysate media in 125 mL Erlenmeyer flasks at 30 °C, 250 rpm for 140 h in 125 mL flasks starting at $OD_{600}$ = 1. The 100 µL samples were taken from each flask at regular intervals for measurements of cell density by spectrophotometer (Safire$^2$; Tecan Group Ltd., Mannedorf, Switzerland), metabolite analysis by high-performance liquid chromatography (HPLC), and washed sam;ples used for lipid quantification. For enzymatic hydrolysis of pretreated Miscanthus biomass, the enzymes cellulase (300 FPU/ml, protein: 85.28 mg/ml) (NS22257, Novozymes, North America, Inc.,

Franklinton, NC, USA) and hemicellulase (1900.8 FXU/ml, protein: 72.8 mg/ml) (NS22244, Novozymes, North America, Inc., Franklinton, NC, USA), and an experimental acetylxylan esterase (AXE) (3.1.1.72) (kindly provided by International Flavors & Fragrances Inc., Cedar Rapids, IA, USA), were used, wherever required.

### 2.3. Alkaline fractionation of biomass components

Alkaline treatment was applied to recover hemicelluloses from M×g biomass. Two fractions, hemicellulose A (HM-A) and B (HM-B), were extracted using a modified alkaline process following protocols for sorghum arabinoxylan and corn fiber gum[13,23]. Biomass (100 g) was stirred in 1 L of 5% NaOH at 85 °C for 2 h, cooled, and centrifuged at 6000×g for 20 min. The supernatant was acidified to pH 4.0–4.5 to precipitate HM-A, collected by centrifugation (10,000×g, 30 min). HM-B was recovered by adding two volumes of ethanol to the remaining supernatant and settling overnight, followed by ethanol washing and vacuum filtration. The fibrous residue from alkaline pretreatment was neutralized to pH 5.5–6.0, filtered, and rinsed with ethanol to obtain a cellulose-rich fraction (CRF). This fractionation process effectively separated the major components of *M*×*g* biomass, yielding distinct hemicelluloses (HM-A and HM-B) and cellulose-rich fractions for further analysis and utilization. Compositional analysis of all the fractions was performed. Parallelly, hydrothermally pretreated (170 °C, 10 min) *M*×*g* biomass was used to demonstrate Miscanthus versatility as a substrate for producing designer high-xylose–acetic acid hydrolysates by enzymatic hydrolysis.

### 2.4. Characterization of pretreated biomass and isolated fractions

#### *2.4.1. Fourier transform infrared (FT-IR) spectroscopy*

FT-IR spectra of raw biomass, pretreated biomass, and isolated fractions were recorded for analyzing their chemical functionalities using the Nicolet iS50 Tri-Detector DTGS MCT-A with Integrated Diamond ATR (Thermo Scientific, Madison, WI, USA), and the method of suppressed total reflection was applied. The spectra were recorded from $4500^{-1}$ to 600 $cm^{-1}$ in transmittance mode at a resolution of 4 $cm^{-1}$ with 64 scans using air as a background.

### *2.4.2. X-ray diffraction (XRD) analysis*

The crystallinity of alkali fractionated samples, including the raw biomass, was performed using a powder X-ray diffraction (XRD) instrument (Bruker, Germany) with a step size of 0.05° maintained at an acceleration voltage of 40 kW and current of 40 mA. The radiation was CuKα anode radiation (λ = 1.54 Å) and a grade range 2θ = 5–60° with a step size increment of 0.03° with a total scan time of 729 seconds. The crystallinity index (CrI) was calculated using the empirical method based on the crystalline and amorphous areas, considering the peaks at 2θ = 18° and 2θ = 22.8°, respectively [21].

### *2.4.3. 2D $^{1}H–^{13}C$ Heteronuclear Single-Quantum Coherence (HSQC) NMR of lignin fractions*

2D $^{1}H–^{13}C$ – HSQC–NMR spectral analysis of lignin rich alkali fractionated samples was performed for semi-quantification of lignin in the samples using a nuclear magnetic resonance (NMR) (Bruker Advance 600 MHz) equipped with a TCI cryoprobe in DMSO-$d_6$ (relaxation delay 1.0 s, acquisition time 3.28 s). 50 mg of lignin samples were placed in 5 mm NMR tubes with 600 µL DMSO-d6 (> 99.5 atom%, D, containing 0.03 vol.% tetramethyl silane). The samples were sealed and sonicated until homogeneity in a Branson 2510 tabletop cleaner (Branson Ultrasonic Corporation, Danbury, CT). Chemical shifts were referenced to the DMSO

peak (δC/δH 39.5/2.5 ppm). Lignin structure and interlinkages were determined from HSQC spectra using Mnova software, following [24]. A semiquantitative analysis of the integrals of the HSQC correlation contour level adjustments for optimal peak separation for relative comparisons presents the data on an S+G+H=100% basis. The S/G ratio was obtained through normalized HSQC integrations.

**2.5. Enzymatic hydrolysis of different biomass fractions**

Separate hydrolysis was performed on cellulose, Hemicelluloses A and B fractions to create diverse hydrolysates. In addition, enzymatic hydrolysis of HMR pretreated Miscanthus was also carried out using different combinations of the enzymes. These approaches allowed for the creation of tailored enzymatic hydrolysate (EH) compositions to meet specific requirements. A regular, high-glucose hydrolysate (HMR-EH1) was prepared alongside the HMR-derived designer, high-xylose hydrolysate (HMR-EH2) to benchmark the engineered yeast's (RT-ADS) performance on Miscanthus hydrolysate, as its response to regular hydrolysate had not been previously assessed. Notably, all five hydrolyses were performed without buffer, based on preliminary results and reports showing no impact on hydrolysate composition, while improving process economics and avoiding ambiguity in fermentation [25].

Pretreated biomass was dried in a convection air oven at 49 °C until the moisture content was below 5% (w/w) and stored in sealed containers. The moisture content of pretreated biomass was measured prior to enzymatic hydrolysis in all cases. Enzymatic hydrolysis employed cellulase (50 FPU/g dry substrate or 14.2 mg protein/g dry substrate), hemicellulase (3.75 mg protein/g dry substrate), and AXE (25% v/v of hemicellulase). Both the moisture content of the biomass and the volume of enzyme solutions were accounted for when calculating the dry

biomass solids loading in hydrolysis. HMR-EH1 and HMR-EH2 hydrolysates were derived from HMR-pretreated Miscanthus using cellulase + hemicellulase, and hemicellulase + AXE, respectively. The fractions obtained from alkali-pretreated biomass, namely cellulose-rich fraction CRF, HM-A, and HM-B, were hydrolyzed by using cellulase (for CRF) and hemicellulase (for HM-A and HM-B). Solids loadings of 10–50% (w/v) were tested to optimize sugar yields. A fed-batch approach was applied above 20% solids, adding biomass in 5% increments every 3 h (Supplementary Information, Table S1). Hydrolysis reactions (50 mL) were run in 125 mL flasks for 96 h at 50 °C (cellulase + hemicellulase) or 60 °C (hemicellulase + AXE) with agitation at 150 rpm. All experiments were conducted in triplicate and samples were withdrawn at different intervals. Five hydrolysates, namely, HMR-EH1 (high glucose - acetic acid or regular hydrolysate), HMR-EH2 (high xylose–acetic acid), CRF-EH (very high glucose), HMA-EH (xylose), and HMB-EH (very high xylose), were produced differing in composition, and C/N ratio, based on the substrate and enzyme combinations.

**2.6. Microbial fermentation of designer hydrolysates for lipid production**

All five hydrolysates (HMR-EH1, HMR-EH2, CRF-EH, HMA-EH, and HMB-EH) were used to assess engineered strain RT-ADS performance. Hydrolysates were prepared by adjusting sugar concentrations to ~35-40 g/L total sugars for fermentation (Supplementary Information, Table S2). Fermentations started with each hydrolysate's native C/N ratio; however, for HMR-EH2 and HMB-EH (C/N 95 and 120, respectively), additional flasks were included at a halved C/N ratio achieved by ammonium nitrate addition to match the 25–60 range of the others. This adjustment enabled accurate comparison of hydrolysate compositions and C/N effects on yeast growth and metabolism. Medium pH was adjusted to 7.0 with 25 mM phosphate buffer.

234 **2.7. Analytical methods**

235 Samples (~0.5 mL) from enzymatic hydrolysis were centrifuged (10,000 × *g*, 10 min),
236 filtered (0.2 μm PTFE), and analyzed for sugars, organic acids, and furan compounds by HPLC
237 (Waters Alliance e2695 Separation module, Waters Corporation, Milford, MA, USA) equipped
238 with a 2414 refractive index detector (Waters Corporation, Milford, MA, USA) and a BioRad
239 Aminex 87H column at 65 °C using 5 mM sulfuric acid as mobile phase at 0.6 mL/min flow rate.
240 Lipid content was measured colorimetrically using the vanillin-phosphoric acid method [26].
241 Briefly, culture pellets centrifuged at 8,000×*g* were hydrolyzed with concentrated sulfuric acid
242 (100 °C, 10 min), reacted with vanillin-phosphoric acid reagent at 37 °C for 15 min in the dark,
243 and absorbance at 530 nm was measured by microplate reader Tecan Infinite M1000 Pro
244 microplate reader (Tecan Group Ltd., Männedorf, Switzerland). Lipid concentration was
245 calculated from a corn oil calibration curve. Fatty acid compositions of extracted lipids were
246 analyzed by GC-FID [27]. Lipids were methylated (2.5% $H_2SO_4$ in methanol, 0.125 mg/mL
247 tridecanoic acid internal standard) at 100 °C for 20 min, extracted with chloroform/water, and
248 injected (5 μL) into an Agilent 7890A GC (HP-INNOWAX column, He carrier). The oven
249 temperature set at an initial hold at 50 °C for 5 min, followed by a ramp of 20 °C/min to 240 °C,
250 with a final hold at 240 °C for 30 min. Fatty acid methyl ester percentages were quantified from
251 peak areas relative to the internal standard.
252
253 **2.8. Data Analysis**
254 All analyses, enzymatic hydrolyses, fermentations, and subsequent tests were performed
255 in triplicate for reproducibility. Statistical differences in sugar recovery at varying solid loadings
256 were evaluated by analysis of variance (ANOVA) followed by Tukey's honest significant

difference (HSD) test ($p \leq 0.05$) using Minitab® Statistical Software version 21 (Minitab® LLC, 2021). Significant differences between mean values are indicated by distinct letters.

## 3. Results and Discussion

### 3.1. Fractionation of M×g components and their chemical composition

Compositional analysis of raw M×g depicted 36.4 ± 3.3% glucan, 20.4 ± 1.9% xylan, and 20.8 ± 1.2% lignin (acid-insoluble) (Table 1). These values align closely with literature reports for miscanthus harvested across different seasons (e.g., 39.9 ± 1.2% glucan, 28.6 ± 1.1% xylan, 20.6 ± 0.2% acid-insoluble lignin confirming compositional representativeness despite known seasonal variability [8]. Carbohydrate fractions in lignocellulosic biomass are embedded in a highly recalcitrant matrix through strong inter/intra-molecular hydrogen bonding, van der Waals forces, limiting the downstream conversion for fuels, chemicals, and materials [28]. However, hemicelluloses are a major barrier to cellulose hydrolysis, but alkali treatment effectively fractionates hemicellulose by cleaving ester linkages with lignin. Thus, in this study, using a modified alkaline method, yields of 55.1 ± 4.3% cellulose-rich fraction (CRF), 14.5 ± 3.2% hemicellulose A (HM-A), and 6.3 ± 2.7% hemicellulose B (HM-B) were obtained (Table 1), consistent with Qiu et al. who reported 13.4 to 16.5% HM-A and substantial cellulose retention in sorghum under similar conditions[13]. They observed lower HM-A yields (13.4 to 16.5%) when processing sorghum under pH 11.5 conditions at 85 °C for 1 h, alongside substantial cellulose retention (35.4 to 46.7% CRF). In a similar report, sequential alkaline extraction in ryegrass removed amorphous hemicelluloses, balancing hemicellulose removal and cellulose preservation [29]. In similar studies, sweet sorghum bagasse yielded 33.3% hemicellulose using 12% NaOH at 80 °C for 4 hours [30]. The yield of hemicellulose from beechwood and agba wood was 39.7% and

36.7%, respectively, when treated with 10% NaOH at 60 °C overnight, while African rosewood yielded 45.5% under the same conditions, indicating biomass-specific variations [31]. Eucalyptus sawdust achieved 42% hemicellulose with 20% NaOH at 100 °C for 1 h, suggesting higher alkali concentration and temperature can offset shorter treatment times [32].

The CRF contained 53.9 ± 4.3% glucan and 15.9 ± 2.1% xylan, with lignin at 9.5 ± 1.2% (AIL) and 1.1 ± 0.0% (ASL), and no detectable ash (Table 1). HM-A had low glucan (2.3 ± 0.4%), moderate xylan (20.6 ± 3.2%), and the highest lignin (39.7 ± 3.4% AIL, 4.3 ± 0.1% ASL). HM-B was rich in xylan (55.8 ± 4.5%), with low glucan (19.8 ± 3.2%) and minimal lignin (3.3 ± 0.8% AIL, 2.2 ± 0.0% ASL). All fractions had minimal acetic acid (0–0.5%) and no ash. Prior studies indicate that using alkaline substances like NaOH and KOH is the favored approach for extracting and dissolving hemicellulose fractions[13,23]. Hemicelluloses are connected via phenolic or non-phenolic ester linkages; additionally, they are crosslinked by diferulic ester-bridges[3]. Alkaline agents break hydrogen and ester bonds, causing cellulose swelling and reduced crystallinity[12,13]. Therefore, alkaline treatment disrupts complex structures, releasing hemicelluloses by targeting these linkages[33]. It also dissolves lignin via phenolic group deprotonation, increasing their negative charge and dispersion[34]. Acidification of the hydrolysate reprotonates phenolic groups, causing lignin to precipitate[35]. Adding ethanol reduces solution polarity, disrupting hemicellulose hydration layers, leading to aggregation and precipitation[36].

Hydrothermal pretreatment, on the other hand, dissolves xylan due to hemicellulose's amorphous nature and releases organic acids like acetic acid, making the environment slightly acidic [37]. This treatment increases cellulose susceptibility to hydrolysis and degrades hemicellulose effectively; however, it only partially degrades the lignin. HMR-pretreated biomass showed a slight decrease in glucan, significant xylan reduction, and minor lignin loss,

303 with altered lignin structure. Lignin, along with the covering the cellulose, also binds with the
304 cellulase so that less enzyme is available to access the cellulose [38].
305
306 **3.2. Designer hydrolysates from isolated M×g fractions and HMR pretreated biomass**
307 Enzymatic hydrolysis of biomass fractions was performed using cellulase, hemicellulase,
308 and AXE to produce five designer hydrolysates (Section 2.5). From HMR-pretreated biomass
309 fed-batch hydrolysis at high solids (30% and 50% w/w) generated two hydrolysates, HMR-EH1
310 and HMR-EH2 (Supplementary Information, Table S1). HMR-EH1, at 50% solids, consists of
311 high-glucose (102.8 ± 6.3 g/L), followed by xylose (84.1 ± 4.2 g/L), and acetic acid (8.2 ± 1.2
312 g/L), total sugar concentration was about 25% lower (*p* value = 0.00) at 40% solid loading, i.e.,
313 88.0 ± 1.2 g/L of glucose, 61.6 ± 3.2 g/L of xylose (Supplementary Information, Fig. S1A).
314 HMR-EH2 on the other hand at maximum achievable solid loading of 30%, resulted in a high-
315 xylose (38.7 ± 3.9 g/L) content followed by glucose (32.2 ± 3.2 g/L), acetic acid (5.1 ± 1.5 g/L)
316 (Supplementary Information, Fig. S1B). HMR-EH2 showed a higher xylose-to-glucose (X/G)
317 ratio (1.2:1) than HMR-EH1 (X/G = 1:0.8). These characteristics make HMR-EH2 particularly
318 valuable for evaluating the performance of engineered microorganisms designed to prefer or co-
319 utilize xylose and acetic acid apart from glucose, as well as for assessing their acetic acid
320 tolerance in real-hydrolysates [16,18]. Yanase et al. engineered *Zymomonas mobilis* for xylose
321 catabolism to convert mixed sugars from wood hydrolysate to ethanol at 89.8% theoretical yield
322 in 72 h [17].
323 CRF is an additional valuable cellulose-rich product in the hemicellulose isolation
324 process, which can be efficiently hydrolyzed to produce glucose-rich hydrolysate (CRF-EH) with
325 reduced enzyme requirements as compared to the HMR pretreated *M×g* biomass due to its high

glucan content (Table 1). Delignified and low in hemicellulose, CRF is highly digestible by cellulase, yielding up to 127.7 ± 7.2 g/L glucose at 30% solids, outperforming other HMR (HMR-EH1, HMR-EH2) hydrolysates (Table 2). CRF-EH contains moderate xylose (33.9 ± 4.2 g/L) and no acetic acid. It is noteworthy that the combination of high glucose yield and reduced enzyme loading may improve the economics of the enzymatic hydrolysis step, although the overall economic viability of the integrated process will require comprehensive techno-economic and life-cycle assessments following further process optimization.

The hydrolysates HMA-EH and HMB-EH exhibited markedly higher xylose concentrations relative to glucose, reflecting the predominance of hemicellulose over cellulose in these fractions. The disparity in xylose yields between these hydrolysates can be attributed to the significant difference in their xylan content, with HM-A containing 20.6 ± 3.2% xylan and HM-B 55.8 ± 4.5% (Table 1). Notably, HMB-EH demonstrated a higher glucose concentration compared to HMA-EH, which correlates with the elevated glucan content in the HM-B fraction. Both hydrolysates contained minimal acetic acid, a favorable characteristic as elevated acetic acid levels can impede fermentation processes. These results suggest that both hydrolysates, particularly HMB-EH, could be valuable for processes that utilize xylose, such as the production of biofuels or biochemicals using xylose-fermenting microorganisms. In a study, engineered *Saccharomyces cerevisiae* strain SR8A6S3-CDT-2-GH43-2/7 co-utilized xylo-oligosaccharides, xylose, and acetate for ethanol production, achieving 60% higher ethanol yields compared to the control strain when fermenting hemicellulosic hydrolysates [18]. Recently, researchers developed a cost-effective strategy for producing lactic acid from glucose and xylose using the acid-tolerant yeast *Issatchenkia orientalis*. By engineering the strain SD108XL and implementing a self-buffering fermentation approach, 67 g/L of lactic acid was produced from 73 g/L of glucose and

40 g/L of xylose, simulating the sugar composition of sorghum biomass hydrolysates [39]. In another recent study, *Yarrowia lipolytica* was engineered for efficient lipid production solely from xylose; however, the performance of the engineered strain was not assessed in the actual 'only xylose' hydrolysate [40]. Interestingly, these findings demonstrated a highly selective approach for the preparation of designer hydrolysate with customized sugar compositions for a particular microbial host from an M×g bioenergy crop following a low-severity alkali method. This approach provides significant versatility in biorefinery processes, allowing for the tailored production of fermentation substrates to meet diverse biotechnological needs.

### 3.3. Microbial lipid production from designer hydrolysates

*R. toruloides* preferentially utilizes glucose over xylose in hydrolysate-based media. Glucose was rapidly depleted (20–68 h) across all hydrolysates, while xylose utilization was slower, extending over 140 h, reflecting *R. toruloides*' preferential glucose uptake and catabolite repression (Fig. 1). High-glucose hydrolysates (HMR-EH1, HMR-EH2, HMR-EH2*, and CRF-EH) showed steep initial glucose decline (0–44 h), followed by xylose co-utilization; HMR-EH2* exhibited faster xylose depletion, likely due to low C/N enhancing pentose catabolism but diverting to non-lipids. Low-glucose, xylose-rich streams (HMA-EH, HMB-EH, HMB-EH*) depleted glucose by 20 h, with HMA-EH/HMB-EH* nearly exhausting xylose, unlike HMB-EH (residual xylose, possible arabitol diversion); overall, hydrolysate design tunes hexose/xylose metabolism balance.

Xylose metabolism is less efficient under low nitrogen conditions. *R. toruloides* 880 has a non-canonical xylose metabolism that goes through D-arabitol and ribulose. Under medium to high nitrogen conditions, a large portion of xylose-derived carbon is diverted toward arabitol

production instead of cell mass or lipid synthesis [26]. This observation aligns with the reduced xylose utilization rate when the organism grows on hydrolysate [20,41]. The effectiveness of lipid accumulation in oleaginous yeasts is fundamentally determined by the transition between two distinct metabolic phases. During cell growth, a low C/N ratio (typically < 30) is required to produce structural proteins, enzymes, and nucleic acids. Under these nitrogen-rich conditions, high intracellular AMP levels maintain a high flux through the TCA cycle, prioritizing biomass doubling over carbon storage. In contrast, the lipid synthesis phase is induced by a high C/N ratio (typically > 60) in which nitrogen becomes the limiting nutrient. This constraint causes a metabolic shift defined by a decrease in AMP levels and the subsequent activation of ATP-citrate lyase (ACL), which redirects carbon flux to the production of triacylglycerols [42]. While our results for HMR-EH2 (C/N 120) are consistent with the conventional model of nitrogen starvation-induced lipogenesis, results for HMB-EH (C/N 95) indicate that an excessively high ratio can be detrimental. A C/N ratio of 95 resulted in a decrease in both growth and lipid output, indicating a state of over-starvation in which the cell lacks the essential enzymatic machinery for carbon uptake and lipid synthesis. Conversely, HMB-EH* performed best at a C/N ratio of 48, providing sufficient nitrogen to build biomass while maintaining effective lipogenic metabolism and xylose utilization. The hydrolysates derived from different biomass fractions and different C/N ratios exhibited distinct sugar profiles and corresponding effects on lipid accumulation (Table 2 and Supplementary information Table S2). HMR-EH1 (C/N ~45) supported robust growth (OD 56.8), 0.11 g/g lipid yield, and coproduction of arabitol, suggesting altered pentose phosphate pathway flux through D-arabitol. CRF-EH had a lower C/N ratio (33) and a higher glucose to xylose ratio (4:1) than HMR-EH1 but showed a lower lipid yield (0.09 g/g) possibly due to higher nitrogen favoring growth (OD 66.4) over lipid accumulation (Supplementary

Information Table S2). HMR-EH2 hydrolysate with a high C/N (120) enhanced lipid accumulation, while lowering C/N to 60 (HMR-EH2*) reduced lipid yield to 0.05 g/g despite similar cell densities (~OD 49). This indicates nitrogen limitation shifts carbon to lipids, the traditional understanding of nitrogen starvation and lipid accumulation in oleaginous yeasts. Conversely, HMB-EH* hydrolysate showed higher lipid yield (0.11 g/g) and cell density (OD 88.5) at lower C/N (48), with arabitol co-production, whereas higher C/N (95) (HMB-EH) reduced both lipid and growth with no arabitol. This striking difference indicates that, for the HMB-EH hydrolysate, a C/N of 95 was perhaps too nitrogen-limited, constraining both growth and lipid biosynthesis. The lower C/N of 48 was likely more balanced, resulting in robust growth, efficient lipid accumulation, and arabitol co-production. These findings demonstrate that optimizing higher C/N ratios is not always beneficial. Instead, there appears to be an "optimal nitrogen window" that varies depending on the hydrolysate. This is likely due to the specific composition of each hydrolysate, including unquantified trace nutrients or inhibitors that behave differently under varying nitrogen levels. Therefore, to increase lipid yields from *Rhodotorula*, it is critical to thoroughly characterize each hydrolysate batch. Tailored nutrient supplementation strategies should then be applied accordingly. The successful utilization of xylose by engineered *R. toruloides* in a high-xylose hydrolysate demonstrates that xylose-rich hydrolysates are an ideal substrate for evaluating the efficiency of microorganisms engineered for high lipid synthesis and xylose utilization. This highlighted the importance of producing designer hydrolysates for further optimizing microbial lipid production and adapting the yeast for lipid accumulation by xylose metabolism. In a recent study, *R. toruloides* 880-ADS grown on glucose-rich oilcane hydrolysate yielded about 0.10 g/g lipid [41]. In another report, *Aureobasidium melanogenum* P10 produced 0.06 g/g lipid on corncob-derived xylose hydrolysate [43]. Designer hydrolysates enable systematic

evaluation and adaptation of microbial performance, providing a valuable platform to assess genetically engineered strains designed for glucose-xylose co-utilization or exclusive xylose utilization.

Table 2 shows a cumulative lipid yield of 32.1 g/kg raw biomass from CRF-EH, HMA-EH, and HMB-EH, exceeding that from HMR-EH2 (29.6 g/kg), likely due to higher sugar recovery from the isolated fractions. The highest lipid yield (41.7 g/kg) was obtained with HMR-EH1, possibly supported by its high acetic acid content (Table 2). Lipid yields were comparable to literature reports, e.g., 47.6 g/kg Miscanthus biomass with *R. toruloides* Y-27012/Y-6987 [8], 35 g/kg olive prunings with *Y. lipolytica* [5], and 56 g/kg corncob with *R. taiwanensis* [44]. Higher corncob performance likely reflects its lower recalcitrance and lignin content versus perennial Miscanthus.

Fatty acid profiles of lipids from seven designer hydrolysates showed characteristic R. toruloides composition, dominated by oleic acid (C18:1; 53–62%), with palmitic (C16:0; 10.7–18.7%) and linoleic (C18:2; 9.7–24.2%) acids prominent (Fig. 2)[41]. HMR-EH2 had the highest unsaturation (24.2% C18:2, 1.71% C16:1, low 3.18% C18:0), likely from optimized C/N ratio suppressing saturated fats. Xylose-rich HMA-EH/HMB-EH yielded similar profiles (C16:0 ≈18.5–18.7%, C18:1 ≈53–54%); glucose-rich CRF-EH/HMR-EH1 maximized C18:1 (62%) with low PUFAs, indicating hexose-driven Δ9-desaturation [45]. Myristic acid (C14:0) was higher in xylose streams (0.90–0.93% vs. 0.51–0.67%), marking pentose catabolism. These substrate-specific fatty acid signatures demonstrate that designer hydrolysates can modulate lipid unsaturation and chain length distribution while maintaining compositions suitable for biodiesel production (high C18:1 content), with HMR-EH2* suggesting further tailoring potential through hydrolysate conditioning.

### 3.4. Characterization of lignin in enzymatic hydrolysis residues

Enzymatic hydrolysis of substrates obtained after HMR pretreatment and alkaline fractionation of M×g biomass yielded substantial residual solids with considerably high lignin content highlighting lignin valorization potential in biorefineries. Compositional analysis revealed that native M×g contained 22.5% lignin. HMR pretreatment does not facilitate the lignin solubilization, retaining 20.4% lignin in pretreated biomass, which was distributed into two fractions, i.e., HMR-EH1-residue, 18.5 ± 1.3%, and HMR-EH2-residue, 31.2 ± 1.5% (Supplementary Information, Table S3).Whereas, alkaline-ethanol treatment attributes in significant dissolution of lignin fraction resulting variable solid recoveries, i.e., 55.1% (CRF), 14.5% (HM-A) and 6.3% (HM-B) substrates. Table S1 (Supplementary Information) depicted the lignin content in leftover enzymatic residue for each fraction. For instance, HMA-EH-residue contained highest amount of lignin 85.7% followed by HMB-EH-residue (73.7%), and CRF-EH-residue (11.7%). Low lignin in CRF-EH-residue could be due to residual cellulosic material. Further, presence of high lignin content in HMA-EH-residue could contribute to its suitability of downstream lignin conversion technologies of value addition. Structural characterization of lignin residues obtained after alkaline fractionation was performed by 2D $^{1}H–^{13}C$ HSQC-NMR. Figure 2 displays the aromatic, aliphatic side chains, and C–O–C interlinkages within the lignin macromolecule. Primary cross-signals for two lignin samples were identified in the spectrum. Alkaline pretreatment led to cleavage of -C–O–C linkages and increased aliphatic side chain signals, evident in HSQC regions for α, β, γ-protons of p-hydroxyphenyl (H), guaiacyl (G), and syringyl (S) units. Lignin is an amorphous polymer of cross-linked phenylpropanoids: coniferyl alcohol (guaiacyl, G), sinapyl alcohol (syringyl, S), and 4-hydroxycinnamyl alcohol (p-hydroxyphenyl, H), linked by ether (β–O–4, α–O–4) and carbon-carbon (β–β, β–5, β–1, 5–5)

bonds (Fig. 3). Reductions in β-O-4 and 4-O-5 linkages correspond to alkaline cleavage, while C–C linkages like β–β increased, consistent with reported mechanisms [46]. Cross-peak assignments follow a previous report [47]. Solvent (DMSO) peaks appeared at $\delta_C/\delta_H$ 40.2/2.5 ppm; methoxy (–OCH3) at 53.1/3.1 ppm. Aliphatic regions revealed prominent β–O–4′ (Aα), β–β (Bα), β–5 (Cα) cross peaks at $\delta_C/\delta_H$ 71.6/4.85, 84.7/4.65, and 86.83/5.42 ppm, respectively. The β-positions of β-aryl ether (β-O-4) ($A_\beta$), resinol (β–β) ($B_\beta$), and phenylcoumaran (β-5) ($C_\beta$), demonstrated the contour plot at chemical shifts nearby $\delta_C/\delta_H$ 86.1/4.05 ($A_\beta$ for syringyl subunits), 83.4/4.33 (Aβ for G), 53.3/3.05, and 52.4/3.45 ppm, respectively. The chemical shift for γ-substituted β-O-4 ($A_\gamma$), β–β ($B_\gamma$), and β-5 ($C_\gamma$) linkages appeared around $\delta_C/\delta_H$ 59.5/3.69, 71.0/4.16–3.79, and 62.3/3.70 ppm, respectively. HMA-EH lignin showed a dissociated structure with reduced β-O-4, β-β, and β-signals.

Quantification indicated β-O-4 bonds at 54.1/100 Ar, confirming ether bond cleavage during alkaline processing. Aromatic HSQC contours showed lignin moiety distributions, syringyl (S), guaiacyl (G), p-hydroxyphenyl (H), within $\delta_C/\delta_H$ 100–150/5.5–8.5 ppm [48]. Contours signal around $\delta_C/\delta_H$ (6.48-6.90)/ (104-109) assigned for $S_{2/6}$. Some oxidized forms of syringyl (S'), ferulic acid (FA), and *p*-coumaric acid (*p*-CE) were also seen in lignin macromolecules. The small presence of *p*-hydroxyphenyl (H) lignin linkages could also be seen in both lignin plots. Guaiacyl (G) lignin subunits exhibited broad correlations due to $C_2$–$H_2$ ($\delta_C/\delta_H$ 113.0/6.2 ppm), $C_5$–$H_5$ ($\delta_C/\delta_H$ 114.6/6.8 ppm), and $C_6$–$H_6$ ($\delta_C/\delta_H$ 116.2/6.7 ppm) for $G_2$, $G_5$, and $G_6$ δC/δH positions and were well distributed in HM and alkali lignin samples. $G_5$ (6.8-6.5/114.6-112.7) contours overlap with $G_6$, ferulate (FA), and *p*-coumarate (*p*CA) and could be observed by signal presence around 6.5-6.3/113.8-114.7, respectively. The peak at $\delta_C/\delta_H$ 7.4/130.7 chemical shifts correspond to $pCA_{2/6}$ and $pCA_{3/5}$. FAα and FAβ correlations coincide with *p*CAα and *p*CAβ,

487 respectively, at positions 145.2/7.4 ppm and 122.2/6.7 ppm. Furthermore, a high number of
488 C−O−C interunit linkages, i.e., β–O–4 (∼54 %) and 4–O–5 (∼5 %), were preserved. Among
489 C−C bonds, ∼39 % β–β and ∼2 % β–5 linkages held together the three phenylpropanoids.
490 Aromatic HSQC regions indicated S dominance (68.7%), G 29.6%, and H 1.7% units with an
491 S/G ratio of 2.3, consistent with typical lignin structures. The preserved interunit linkages
492 support potential for valorization as feedstock for polymers, adhesives, and carbon fibers [47].
493

494 **3.5. Chemical characterization of pretreated biomass and isolated fractions**

495 To analyze the chemical structure of the isolated CRF, HM-A, and HM-B fractions of
496 M×g, along with HMR pretreated and raw M×g samples, FT-IR spectra were recorded (Fig. 4).
497 Residues from enzymatic hydrolysis of HM-A and HM-B were also included to assess the
498 impact of component removal on remaining solids. Literature describes absorption bands for
499 pure cellulose and plant cell wall components[49]. Native M×g showed two spectral regions: 3500–
500 2800 $cm^{-1}$ (O–H and C–H stretching vibrations) and 1700–850 $cm^{-1}$, attributed to cellulose,
501 hemicellulose, and lignin. All samples exhibited a broad peak near 3300 $cm^{-1}$ from aromatic and
502 aliphatic hydroxyl groups in hemicellulose and lignin, intensified in raw biomass, HM-B, HM-A,
503 and HM-EH residues[50]. This peak disappeared in CRF and HMR-pretreated biomass, reflecting
504 hemicellulose and lignin removal and hydrogen bond disruption. However, HM-A and HM-B
505 EH residues showed intensified peaks due to hemicellulose removal and lignin enrichment.
506 The 2920 $cm^{-1}$ peak corresponds to −CH bond deformation of $-CH_2$ groups in methoxy,
507 methyl, and methylene groups [51] . Lignin peaks between 1627–1424 $cm^{-1}$ arise from asymmetric
508 C–H deformations in aromatic lignin subunits [49]. The aromatic ring vibrations of lignin appeared
509 at 1591 $cm^{-1}$ (–C=C stretching), 1504 $cm^{-1}$ (antisymmetric –COO− stretching), 1464 $cm^{-1}$ (C-O-

C stretching), and 1424 $cm^{-1}$ get intensified in HMA-EH and HMB-EH residues due to high lignin content. Cellulose bands at 1200–898 $cm^{-1}$ correspond to C–O, O–H, C–C, C–OH, and C–O–C vibrations. Hemicellulose bands ranged from 1420–890 $cm^{-1}$, stronger in HM-A and HM-B fractions [50]. Peaks between 1070–1030 $cm^{-1}$ indicate xylose in hemicellulose. HM-B showed stronger 897 and 1031 $cm^{-1}$ peaks than HM-A, reflecting its higher hemicellulose content (Table 1). The CRF spectrum showed reduced intensities near 1500–1424 $cm^{-1}$ and 1600 $cm^{-1}$, indicating significant cellulose enrichment because of hemicellulose and lignin separation during alkali pretreatment. Hemicellulose consists of acetyl functionality in its chemical structure and shows an acetyl stretching ($–OCH_3$) at 1700 $cm^{-1}$, which reduced in CRF-EH and HM-EH residues, reflecting removal or alteration of hemicellulose during alkaline pretreatment and enzymatic hydrolysis.

Crystalline cellulose in lignocellulosic biomass is highly ordered and tightly bound with other cell wall components, forming a resistant lignin-carbohydrate matrix. The crystallinity index (CrI) is a key factor affecting biomass properties and digestibility. During alkaline treatment, NaOH swells the biomass and penetrates cellulose, disrupting hydrogen bonds and altering the crystal structure [12]. XRD diffractograms of raw biomass, HMR pretreated, HM-A, HM-B, and CRF fractions (Fig. 5) revealed crystalline peaks characteristic of cellulose I at $2\theta \approx 22.8°$, with weaker overlapping peaks at 15.3°, 16.4°, 20.5°, and 22.7°, corresponding to various lattice planes (101, 021, 002, and 040). Alkaline treatment solubilizes hemicellulose and amorphous cellulose, marginally increasing CrI in cellulose-rich fractions like CRF, consistent with observations in other biomass such as cocksfoot grass [52]. Hemicellulose, a branched heteropolymer with irregular amorphous structure, shows a broad diffraction peak at $2\theta \approx 18.7°$ attributed to xylan. Shifts and intensity reductions near 20.4° indicate carbon structural changes

in hemicellulose fractions (HM-A, HM-B), supported by composition and FTIR data [50]. However, alkali pretreatment slightly modifies the native crystalline structure, indicating deconstruction and new crystal plane formation. Increased CrI values in CRF result from dissolution of amorphous lignin and hemicellulose during treatment, enhancing enzymatic digestibility via an open matrix that improves cellulase accessibility [29].

## 4. Conclusions

This study demonstrated a novel low-severity alkaline processing strategy to selectively fractionate hemicelluloses (HM-A, HM-B), cellulose-rich fraction (CRF), and lignin from miscanthus. Among five designer hydrolysates, HMB-EH was xylose-rich (173.4 ± 4.6 g/L) while CRF-EH was glucose-rich (127.7 ± 7.2 g/L). Lipid yield from these hydrolysates using *Rhodotorula toruloides* 880-ADS ranged from 0.05 to 0.12 $g/g_{sugar}$. From biomass fractionation approach about 32.1 g lipid/kg raw miscanthus was achieved, however, with hydrothermally (HMR) pretreated miscanthus, 29.6 g/kg (HMR-EH2) and 41.7 g/kg (HMR-EH1) lipid yield were achieved. High lignin (73.7 to 85.7%) in spent residues support sustainable lignin valorization. These findings provide a baseline for future scale up studies under controlled bioreactor system, reduced inhibitors, and further optimization of C/N ratios, e.g., 120 for glucose-rich HMR-EH2 for higher lipid accumulation, and C/N 48 for HMB-EH biomass/lipid/arabitol balance. This work establishes a holistic integrated biorefinery platform yielding tailored sugar streams for diverse biochemical conversion. To comprehensively evaluate the economic and environmental performance of the integrated biorefinery process, future work should include techno-economic analysis and life cycle assessment of the optimized process, incorporating fermentation productivity, nutrient utilization, and product recovery.

## CRediT authorship contribution statement

**Shuchi Singh**: Writing – original draft, Writing – review & editing, Visualization, Validation, Methodology, Investigation, Data curation; **Tirath Raj**: Writing – review and editing, Data curation, Investigation; **Joshua Ye**: Writing – review & editing, Data curation, Investigation; **Sujit Sadashiv Jagtap**: Writing – review & editing; **Cindy Yang:** Writing – review & editing, Data curation, Investigation, **Christopher V. Rao**: Resources; Supervision; Writing – review and editing, **Vijay Singh**: Conceptualization, Supervision, Writing – review and editing, Funding Acquisition.

## Declaration of Competing Interest

The authors declare that they have no known competing financial interests or personal relationships that could have appeared to influence the work reported in this paper.

## Acknowledgments

The authors are thankful to the DOE Center for Advanced Bioenergy and Bioproducts Innovation for providing financial support for this research. This work was funded by the DOE Center for Advanced Bioenergy and Bioproducts Innovation (U.S. Department of Energy, Office of Science, Biological and Environmental Research Program under Award Number DE-SC0018420). Any opinions, findings, and conclusions or recommendations are those of the authors and do not necessarily reflect the views of the U.S. Department of Energy. Authors are thankful to Prof. Eric Sacks and Brent Daniel Berns for providing the raw Miscanthus biomass. The authors express gratitude to Novozymes North America and International Flavors &

Fragrances Inc. for supplying the enzymes used in this study. The inclusion of specific product names is intended solely for scientific clarity and does not constitute an endorsement or recommendation by the U.S. Department of Agriculture. The USDA maintains its commitment as an equal opportunity provider and employer. The authors gratefully acknowledge Dr. Dean L. Olson (School of Chemical Sciences) for NMR analysis and the Materials Research Laboratory Central Research Facilities at the University of Illinois at Urbana-Champaign for access to and assistance with XRD, NMR, and FT-IR analyses. The authors acknowledge Kristen Eilts for conducting the HPLC analyses.

**Supplementary data**

E-supplementary data of this word can be found in online version of the paper.

**Data availability statement**

The authors declare that all data supporting the findings of this study are available within the paper. For any further data requests, please reach out to the corresponding author. Your inquiry will be promptly addressed to enhance the understanding of the research.

## References


G. Aslan-Sungur, N. Boersma, C. E. Moore, E. Heaton, C. J. Bernacchi and A. Vanloocke, *GCB Bioenergy*, DOI:10.1111/gcbb.70012.

J. Kim, J. Ko, Y. Lee, H. Lee, S. Jeong, J. Yoo, S. A. Lee, G. Gong, Y. W. Suh, S. M. Lee, J. Han and S. Hwangbo, *Chemical Engineering Journal*, DOI:10.1016/j.cej.2025.161171.

J. Rao, Z. Lv, G. Chen and F. Peng, 2023, preprint, DOI: 10.1016/j.progpolymsci.2023.101675.

M. H. Cheng, L. Sun, Y. S. Jin, B. Dien and V. Singh, *Bioresour. Technol.*, 2020, **308**, 123275.

B. Dias, R. M. Rodríguez-Jasso, I. Belo and M. Lopes, *Chem. Eng. Sci.*, DOI:10.1016/j.ces.2024.121150.

A. Lorenci Woiciechowski, C. J. Dalmas Neto, L. Porto de Souza Vandenberghe, D. P. de Carvalho Neto, A. C. Novak Sydney, L. A. J. Letti, S. G. Karp, L. A. Zevallos Torres and C. R. Soccol, 2020, preprint, DOI: 10.1016/j.biortech.2020.122848.

V. B. Agbor, N. Cicek, R. Sparling, A. Berlin and D. B. Levin, *Biotechnol. Adv.*, 2011, **29**, 675–685.

S. Banerjee, B. S. Dien, K. K. Eilts, E. J. Sacks and V. Singh, *Chemical Engineering Journal*, DOI:10.1016/j.cej.2024.150117.

M. H. Cheng, S. Singh, A. N. Carr Clennon, B. S. Dien and V. Singh, *Bioresour. Technol.*, 2023, **380**, 129104.

K. Tanaka, T. Yukawa, T. Bamba, M. Wakiya, R. Kumokita, Y. S. Jin, A. Kondo and T. Hasunuma, *Appl. Microbiol. Biotechnol.*, 2025, **109**, 30.

T. A. L. Silva, L. H. R. Varão and D. Pasquini, in *Handbook of Biomass*, eds. S. Thomas, M. Hosur, D. Pasquini and C. Jose Chirayil, Springer Nature Singapore, Singapore, 2024, pp. 105–142.

S. Singh, S. T. P. Bharadwaja, P. K. Yadav, V. S. Moholkar and A. Goyal, *Ind. Eng. Chem. Res.*, DOI:10.1021/ie502339q.

S. Qiu, M. P. Yadav and L. Yin, *Food Chem.*, 2017, **230**, 225–233.

S. C. Sun, P. F. Wang, X. F. Cao, S. N. Sun and J. L. Wen, *Ind. Crops Prod.*, DOI:10.1016/j.indcrop.2021.114101.

L. Sun and Y. S. Jin, *John Wiley and Sons Inc*, 2021, preprint, DOI: 10.1002/biot.202000142.

K. L. Dunn and C. V Rao, *Biotechnol. Bioeng*, 2015, **112**, 2228–2239.

H. Yanase, H. Miyawaki, M. Sakurai, A. Kawakami, M. Matsumoto, K. Haga, M. Kojima and K. Okamoto, *Appl. Microbiol. Biotechnol.*, 2012, **94**, 1667–1678.

62818 D. P. Procópio, J. W. Lee, J. Shin, R. Tramontina, P. F. Ávila, L. B. Brenelli, F. M. Squina, A.
629 Damasio, S. C. Rabelo, R. Goldbeck, T. T. Franco, D. Leak, Y. S. Jin and T. O. Basso, *Sci. Rep.*,
630 DOI:10.1038/s41598-023-46293-8.

63119 S. S. Jagtap, A. A. Bedekar, J. J. Liu, Y. S. Jin and C. V. Rao, *Biotechnol. Biofuels*,
632 DOI:10.1186/s13068-019-1586-5.

63320 W. Woodruff, N. N. Deshavath, V. Susanto, C. V. Rao and V. Singh, *Biotechnology for Biofuels*
634 *and Bioproducts*, DOI:10.1186/s13068-023-02429-6.

63521 J. Sluiter, A. Sluiter, C. Scarlata, D. Templeton, D. Crocker and B. Hames, Determination of
636 Structural Carbohydrates and Lignin in Biomass: Laboratory Analytical Procedure (LAP)
637 (Revised August 2012): Issue Date: 4/25/2008.

63822 S. Zhang, M. Ito, J. M. Skerker, A. P. Arkin and C. V. Rao, *Appl. Microbiol. Biotechnol.*, 2016,
639 **100**, 9393–9405.

64023 M. P. Yadav, D. B. Johnston and K. B. Hicks, *J. Agric. Food Chem.*, 2007, **55**, 6366–6371.

64124 H. Kim and J. Ralph, *Org. Biomol. Chem.*, 2010, **8**, 576–591.

64225 N. N. Deshavath, V. V. Goud and V. D. Veeranki, *J. Environ. Chem. Eng.*, 2021, **9**, 105696.

64326 S. S. Jagtap, A. Deewan, J. J. Liu, H. E. Walukiewicz, E. J. Yun, Y. S. Jin and C. V. Rao, *Appl.*
644 *Microbiol. Biotechnol.*, 2021, **105**, 7411–7425.

64527 S. Do Yook, J. Kim, H. M. Woo, Y. Um and S. M. Lee, *Renew. Energy*,
646 DOI:10.1016/j.renene.2018.07.129.

64728 T. Raj, B. S. Dien and V. Singh, *Chemical Engineering Journal*,
648 DOI:10.1016/j.cej.2024.152657.

64929 S. C. Sun, P. F. Wang, X. F. Cao, S. N. Sun and J. L. Wen, *Ind. Crops Prod.*,
650 DOI:10.1016/j.indcrop.2021.114101.

65130 L. Wei, T. Yan, Y. Wu, H. Chen and B. Zhang, *PLoS One*, DOI:10.1371/journal.pone.0195616.

65231 V. E. Ottah, A. L. Ezugwu, T. C. Ezike and F. C. Chilaka, *Heliyon*,
653 DOI:10.1016/j.heliyon.2022.e09714.

65432 D. Longue Júnior, J. L. Colodette and V. J. Gomes, *Cerne*, DOI:10.1590/s0104-
655 77602010000400001.

65633 S. L. Sun, J. L. Wen, M. G. Ma and R. C. Sun, *Carbohydr. Polym.*,
657 DOI:10.1016/j.carbpol.2012.11.098.

65834 O. Sevastyanova, M. Helander, S. Chowdhury, H. Lange, H. Wedin, L. Zhang, M. Ek, J. F.
659 Kadla, C. Crestini and M. E. Lindström, *J. Appl. Polym. Sci.*, DOI:10.1002/app.40799.

66035 T. Li and S. Takkellapati, *Biofuels, Bioproducts and Biorefining*, DOI:10.1002/bbb.1913.

66136 Z. Liu, P. Fatehi, S. Sadeghi and Y. Ni, *Bioresour. Technol.*, 2011, **102**, 9613–9618.

66237 C. K. Nitsos, K. A. Matis and K. S. Triantafyllidis, *ChemSusChem*,
663 DOI:10.1002/cssc.201200546.

66438 J. K. Ko, Y. Um, Y. C. Park, J. H. Seo and K. H. Kim, 2015, preprint, DOI: 10.1007/s00253-
665 015-6595-0.

66639 Y. G. Lee, N. K. Kang, C. Kim, V. G. Tran, M. Cao, Y. Yoshikuni, H. Zhao and Y. S. Jin,
667 *Bioresour. Technol.*, DOI:10.1016/j.biortech.2024.130641.

66840 I. De La Torre, M. G. Acedos, J. J. Cestero, J. Barriuso and J. L. García, *Microb. Biotechnol.*,
669 DOI:10.1111/1751-7915.70127.

67041 N. N. Deshavath, W. Woodruff, F. Eller, V. Susanto, C. Yang, C. V. Rao and V. Singh,
671 *Bioresour. Technol.*, DOI:10.1016/j.biortech.2024.130594.

67242 S. Papanikolaou and G. Aggelis, 2011, preprint, DOI: 10.1002/ejlt.201100014.

67343 S. S. Song, B. C. Tian, H. Chen, Z. Chi, G. L. Liu and Z. M. Chi, *Renew. Energy*, 2022, **200**,
674 1211–1222.

67544 Z. Miao, X. Tian, W. Liang, Y. He and G. Wang, *Renew. Energy*,
676 DOI:10.1016/j.renene.2020.07.007.

67745 I. R. Sitepu, L. A. Garay, R. Sestric, D. Levin, D. E. Block, J. B. German and K. L. Boundy-
678 Mills, 2014, preprint, DOI: 10.1016/j.biotechadv.2014.08.003.

67946 R. W. Houston and N. H. Abdoulmoumine, *RSC Adv.*, DOI:10.1039/d2ra07787f.

68047 U. P. Agarwal and S. A. Ralph, *Holzforschung*, 2008, **62**, 667–675.

68148 X. Zhou, X. Liu, Y. Zhan, H. Bian, S. Wu, H. Dai, F. Liang, X. Meng, C. Huang, G. Fang and A.
682 J. Ragauskas, *Chemical Engineering Journal*, DOI:10.1016/j.cej.2024.150407.

68349 A. M. Raspolli Galletti, A. D'Alessio, D. Licursi, C. Antonetti, G. Valentini, A. Galia and N.
684 Nassi O Di Nasso, *Journal of Spectroscopy*, DOI:10.1155/2015/719042.

68550 T. Liang and L. Wang, *Bioresources*, DOI:10.15376/biores.12.1.1128-1135.

68651 S. L. Sun, J. L. Wen, M. G. Ma and R. C. Sun, *Carbohydr. Polym.*,
687 DOI:10.1016/j.carbpol.2012.11.098.

68852 S. F. Sun, H. Y. Yang, J. Yang and Z. J. Shi, *Ind. Crops Prod.*,
689 DOI:10.1016/j.indcrop.2022.114654.

690

691

692 **Figure Captions:**

693 **Figure 1**. Sugar consumption, cell density, and lipid production profiles of RT880-ADS grown
694 on (A) HMR-EH1, Enzymatic hydrolysate produced from HMR pretreated *M*×*g* using Cellulase
695 + Hemicellulase, (B) HMR-EH2, Enzymatic hydrolysate produced from HMR pretreated M×g
696 using Hemicellulase + AXE, (C) HMR-EH2*, Enzymatic hydrolysate produced from HMR
697 pretreated M×g using Hemicellulase + AXE at C/N adjusted to half (D) CRF-EH, Enzymatic
698 hydrolysate produced from Cellulose rich fraction (CRF), (E) HMA-EH, Enzymatic hydrolysate
699 produced from Hemicellulose A, (F) HMB-EH, Enzymatic hydrolysate produced from
700 Hemicellulose B. (G) HMB-EH, Enzymatic hydrolysate produced from Hemicellulose B at C/N
701 adjusted to half. All experimental values are mean ± SD (n = 3).

702 **Figure 2.** Composition of fatty acid methyl esters (FAMEs) from lipids extracted by supercritical
703 $CO_2$ from *R. toruloides* 880-ADS cultured in designer Miscanthus hydrolysates. Data shown are
704 means of three technical replicates (n = 3), with error bars representing standard deviation.

705 **Figure 3.** 2D-HSQC NMR contour plots of miscanthus lignin samples. a) Aromatic regions of
706 HM-A lignin fraction, b) aliphatic regions of HM-A lignin, c) aromatic regions of HM-B lignin
707 fraction, d) aliphatic regions of HM-B lignin fraction. Different bonds cross peak signals arising
708 from the condensed lignin present in this sample are indicated on the spectrum and on the
709 accompanied structures of compounds.

710 **Figure 4.** FTIR spectrum of raw M×g, cellulose-rich fraction (CRF), and Hemicellulose (HM-A
711 and HM-B) fractions, HMR pretreated biomass, and residues obtained after enzymatic hydrolysis
712 of HM-A and HM-B fractions.

713 **Figure 5.** XRD diffractogram of native M×g, cellulose-rich fraction (CRF), and Hemicellulose A
714 (HM-A) and Hemicellulose B (HM-B) fraction.

Table 1. Compositional analysis of different biomass fractions

| | Yield (%) | Extractives (%) | Glucan (%) | Xylan (%) | Arabinan (%) | Acetic acid (%) | AIL (%) | ASL (%) | Ash (%) |
|---|---|---|---|---|---|---|---|---|---|
| Raw M×g Biomass | - | 13.5 ± 2.3 | 36.4 ± 3.3 | 20.4 ± 1.9 | 1.6 ± 0.2 | 3.9 ± 0.6 | 20.8 ± 1.2 | 1.5 ± 0.4 | 2.5 ± 0.2 |
| Hydrothermal-Mechanical Refining (HMR) pretreatment | 100 | 18.9 ± 1.8 | 34.2 ± 2.2 | 14.3 ± 2.1 | 1.7 ± 0.2 | 2.9 ± 0.5 | 18.5 ± 2.1 | 1.6 ± 0.2 | 2.8 ± 0.4 |
| *Alkali pretreatment for biomass fractionation* | | | | | | | | | |
| Cellulose-rich fiber (CRF) | 55.1 ± 4.3 | 0.0 ± 0.0 | 53.9 ± 4.3 | 15.9 ± 2.1 | 1.5 ± 0.3 | 0.0 ± 0.0 | 9.5 ± 1.2 | 1.1 ± 0.04 | 0.0 ± 0.0 |
| Hemicellulose A (HM-A) | 14.5 ± 3.2 | 0.0 ± 0.0 | 2.3 ± 0.4 | 20.6 ± 3.2 | 1.9 ± 0.2 | 0.5 ± 0.07 | 39.7 ± 3.4 | 4.3 ± 0.06 | 0.2 ± 0.0 |
| Hemicellulose B (HM-B) | 6.3 ± 2.7 | 0.0 ± 0.0 | 19.8 ± 3.2 | 55.8 ± 4.5 | 4.9 ± 0.3 | 0.5 ± 0.06 | 3.3 ± 0.8 | 2.2 ± 0.02 | 0.0 ± 0.0 |

*AIL, Acid insoluble lignin; ASL, Acid soluble lignin.*

*All experimental values are mean ± SD (n = 3).*

Table 2. Composition of designer hydrolysates and a mass balance for estimating lipid production from all the hydrolysates

| Hydrolysate Type | Solid loading in Enzymatic Hydrolysis (%) | Total sugar yield (%)[#] | Glucose (g/L) | Xylose (g/L) | Arabinose (g/L) | Acetic acid (g/L) | Lipid ($g/g_{sugar}$) | Lipid ($g/Kg_{Raw\ Biomass}$) |
|---|---|---|---|---|---|---|---|---|
| HMR-EH1 | 50 | 68.2 | 102.8 ± 6.3 | 84.1 ± 4.2 | 4.6 ± 0.7 | 8.2 ± 1.2 | 0.11 | 41.7 |
| HMR-EH2 | 30 | 43.6 | 32.2 ± 3.2 | 38.7 ± 3.9 | 2.6 ± 0.4 | 5.1 ± 1.5 | 0.12 | 29.6 |
| HMR-EH2* | 30 | - | 32.2 ± 3.2 | 38.7 ± 3.9 | 2.6 ± 0.4 | 5.1 ± 1.5 | 0.05 | - |
| *Hydrolysis of M×g Fractions after Alkaline Pretreatment* | | | | | | | | |
| CRF-EH | 30 | 68.3 | 127.7 ± 7.2 | 33.9 ± 4.2 | 1.6 ± 0.3 | 0.0 ± 0.0 | 0.09 | |
| HMA-EH | 50 | 90.0 | 13.4 ± 2.4 | 104.8 ± 5.6 | 9.0 ± 0.5 | 1.7 ± 0.8 | 0.10 | 32.1[##] |
| HMB-EH | 50 | 43.8 | 19.5 ± 3.2 | 173.4 ± 4.6 | 6.7 ± 0.4 | 1.6 ± 0.5 | 0.09 | |
| HMB-EH* | 50 | - | 19.5 ± 3.2 | 173.4 ± 4.6 | 6.7 ± 0.4 | 1.6 ± 0.5 | 0.11 | - |

*HMR-EH1, Enzymatic hydrolysate produced from HMR pretreated M×g using Cellulase + Hemicellulase; HMR-EH2, Enzymatic hydrolysate produced from HMR pretreated M×g using Hemicellulase + AXE; CRF-EH, Enzymatic hydrolysate produced from Cellulose-rich fraction (CRF); HMA-EH, Enzymatic hydrolysate produced from Hemicellulose A; HMB-EH, Enzymatic hydrolysate produced from Hemicellulose B.*

***C/N ratio was reduced to half of the initial C/N ratio of original hydrolysates HMR-EH2 and HMB-EH (Ratios are mentioned in Supplementary Information Table S2).*

*[#]Total sugar yield (%) was calculated as: Glucose + xylose + arabinose in hydrolysate (g) / Glucose (glucan × 1.11) + xylose (xylan × 1.14) + arabinose (arabinan × 1.14) in substrate at respective solid loading (g) × 100; where 1.11 and 1.14 are the conversion factors for glucan to glucose and pentose sugars (xylan to xylose, and arabinan to arabinose, respectively, considering anhydrous corrections (Sluiter et al. 2008).*

*[##]Lipid yield reported from hydrolysates of Miscanthus fractions (CRF, HMA, and HMB) is the sum of lipids obtained from CRF, HMA-EH, and HMB-EH. Individual lipid yields from CRF, HMA-EH, and HMB-EH were 26.8 g/Kg Raw Biomass, 2.9 g/Kg Raw Biomass, and 2.4 g/Kg Raw Biomass, respectively.*

*Lipid yields were calculated as grams of lipid produced per gram of sugar consumed, where sugar consumed = (initial glucose + xylose + arabinose) – (residual glucose + xylose + arabinose) at the end of fermentation.*

*All experimental values are mean ± SD (n = 3). Lipid titer data used for yield calculations are provided in Supplementary Information Table S2.*

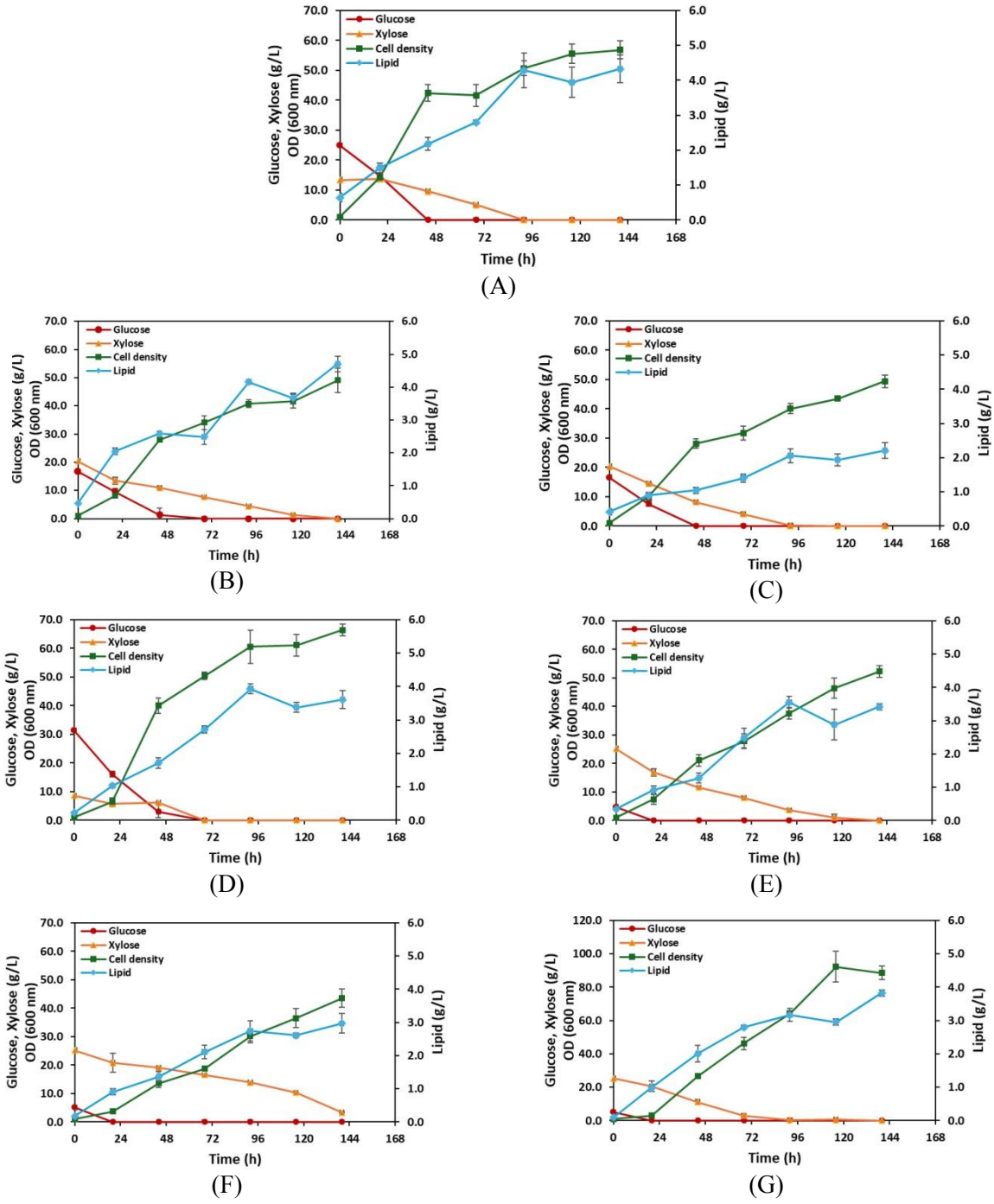


**Figure 1**

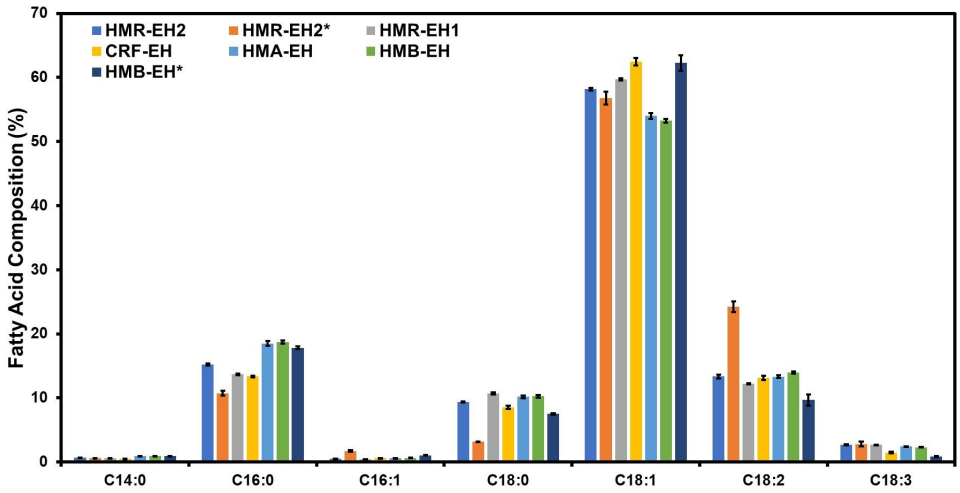


**Figure 2**

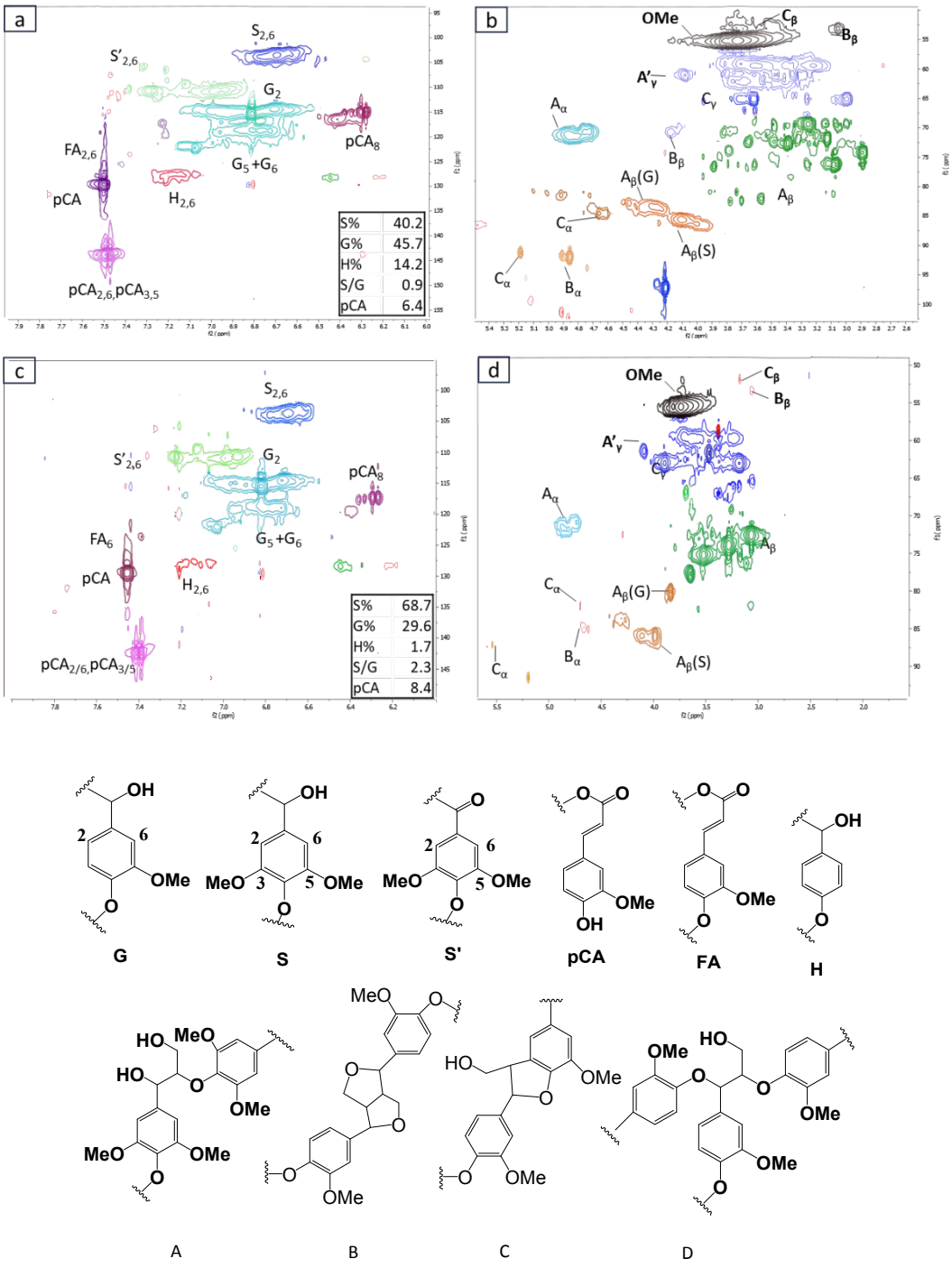


**Figure 3**

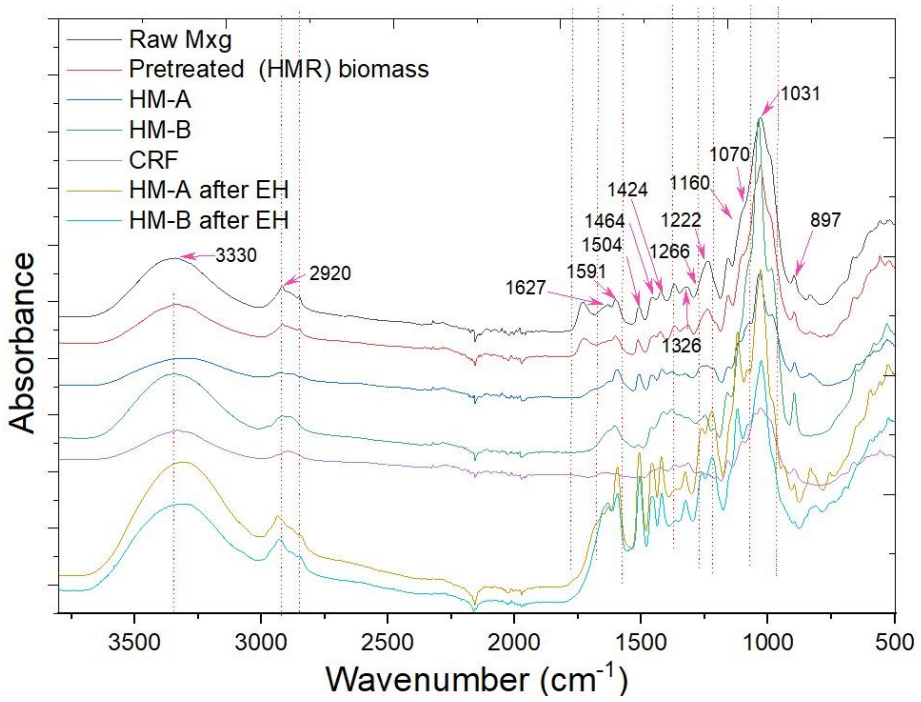


**Figure 4**

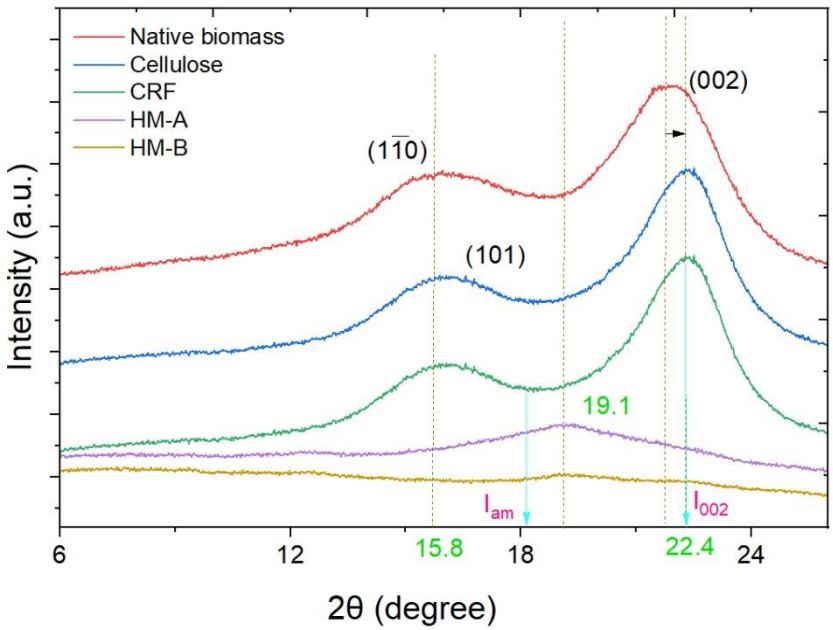


**Figure 5**

**Data availability statement**

The authors declare that all data supporting the findings of this study are available within the paper. For any further data requests, please reach out to the corresponding author. Your inquiry will be promptly addressed to enhance the understanding of the research.